Three-Phase Resonant Switched Capacitor LED Driver With Low Flicker

Ronaldo P. Coutinho, Kleber C. A. de Souza, Fernando L. M. Antunes, *Member, IEEE*, and Edilson Mineiro Sá Jr.

***Abstract*—This paper proposes a light-emitting diode (LED) driver based on a three-phase resonant switched capacitor (SC) converter. The LED lamp employs chip-on-board (COB) technology, as it is possible to achieve high power density. The three-phase structure provides low ripple current and reduced percent flicker. Besides, it does not use electrolytic capacitors, thus, causing the driver lifetime to increase. The converter active switches are turned off under zero current switching (ZCS) and zero voltage switching (ZVS) conditions, as efficiency is consequently increased. LED dimming is also a prominent advantage, what can be obtained by varying the switching frequency. An experimental prototype rated at 216 W has been developed in order to evaluate the performance of the proposed approach, while results are properly presented and discussed. LED dimming is possible as the output power varies from 50% to 100%. Overall efficiency and power factor are higher than 90% and 0.97 over the entire load range, respectively.**

***Index Terms*—Chip-on-board (COB) light-emitting diodes (LEDs), LED driver, reduced flickering, switched capacitor (SC) converters, three-phase converter.**

I. Introduction

LIGHT-EMITTING diodes (LEDs) have been increasingly used in various lighting applications. Due to their intrinsic high luminous efficacy and long lifetime, they have been intensively used in domestic, automotive, industrial, and also in public lighting sectors. At higher power levels, e.g., street lighting and industrial lighting, chip-on-board (COB) LED technology is a prominent choice since LED chips are mounted directly close to each other on a substrate or a circuit board, thus, providing higher power density [1]. Currently, COB LEDs whose luminous efficacy is about 160 lm/W are commercially available [2].

Manuscript received July 6, 2016; revised October 19, 2016 and December 19, 2016; accepted January 13, 2017. Date of publication March 3, 2017; date of current version June 9, 2017. This work was supported in part by the following Brazilian research financing agencies: CNPq, CAPES, FINEP, and FUNCAP.

R. P. Coutinho is with the Federal University of Ceará (UFC), Sobral 62010-560, Brazil (e-mail: ronaldoportela91@gmail.com).

F. L. M. Antunes is with the Department of Electrical Engineering, Federal University of Ceará (UFC), Fortaleza 60440-554, Brazil (e-mail: fantunes@dee.ufc.br).

K. C. A. de Souza and E. M. Sá Jr. are with the Federal Institute of Ceará (IFCE), Sobral 62042-030, Brazil (e-mail: eng.ksouza@gmail.com; edilson.mineiro@gmail.com).

Color versions of one or more of the figures in this paper are available online at http://ieeexplore.ieee.org.

Digital Object Identifier 10.1109/TIE.2017.2677305

The useful life of LEDs is estimated at 50 000 h [3]. However, the useful life of LED drivers is generally limited by the use of conventional electrolytic capacitors, whose useful life is about 10 000 h and depends on the operating temperature [4]. It is also reasonable to state that such devices are not appropriate when considering lifespan extension of LED drivers.

Some research works have shown that excessive percent flicker may cause damage to human health, such as headache, malaise, and even seizures [5], [6]. According to [7], it is necessary to restrict the percent flicker in order to minimize risks to human health. Due to the existence of an ac–dc stage in LED drivers, the flickering frequency is typically rated at twice the ac mains frequency. Therefore the percent flicker occurs at 100 Hz or 120 Hz for 50 Hz or 60 Hz, as it must be restricted to 8% and 10%, respectively [7].

LED drivers can be classified in two types: single-stage [8]–[10] and two-stage drivers [11], [12]. The first class aggregates both power factor correction (PFC) and power control (PC) in a single power converter and usually presents low component count [13]. However, they typically use an output electrolytic capacitor to reduce the ripple current through LEDs, thus, compromising the very useful life of the driver. On the other hand, two distinct converters are responsible for PFC and PC in two-stage drivers. Generally, the PFC stage is designed to provide high output voltage ripple, thus, avoiding the use of electrolytic capacitors. However, the PC stage is supposed to be designed in order to overcome such undesirable ripple [14]. Even though the use of electrolytic capacitors can be avoided, high component count, and reduced overall efficiency are possible drawbacks in this case. When the integrated-stage approach is adopted [15]–[17], the same active switches can be used by both PFC and PC stages, with consequent reduction of component count. However, the circuit complexity generally increases and overall efficiency is reduced since energy flows repeatedly through the circuit. If partial energy processing techniques are used [18]–[20], most of the energy is directly processed by the LEDs as efficiency increases, since only a small amount of the energy flows through the PC stage. However, a bidirectional converter is usually required for the PC stage, thus, bringing increased complexity to the control system. Drivers based on the ripple cancellation converter (RCC) [21]–[23] aim at reducing the redundant energy flow, while the RCC is only supposed to process a small part of the total output power. Some authors refer to such drivers as optimized cascade [24]–[26] ones, where the output current ripple and consequently the percent flicker depend on the accurate functioning of a complex control system, thus implying increased cost.

The use of three-phase drivers in public and industrial lighting is a feasible solution due to the presence of an ac three-phase grid at the power distribution system [27]. It is worth to mention that the instantaneous power in a balanced three-phase converter with unity power factor is constant [28]. Since LEDs present voltage source characteristic, the output voltage V_o is nearly constant, so the output current is. Thus, three-phase drivers come as a prominent solution as it is possible to obtain low ripple current through the LEDs, with consequent reduction of percent flicker.

Unlike single-phase drivers, the ac–dc conversion in three-phase drivers causes the output voltage ripple frequency to be six times higher than the mains frequency [29]. In this case, if the mains frequency is 50 Hz or 60 Hz, flicker will occur at 300 Hz or 360 Hz and should be limited to 24% or 29%, respectively [7]. Since the flickering frequency is higher in three-phase drivers, the percent flicker limit is higher than that for single-phase ones, thus, making them a prominent choice.

A three-phase flyback converter for driving LEDs was proposed in [27]. The converter can operate over a wide input voltage range and employs peak current mode control strategy, which reduces overall costs due to the use of a simple controller. However, appreciable losses exist due to the inductance of the flyback transformer. A three-phase converter with galvanic isolation based on loss-free resistors (LFRs) for high-brightness LEDs was introduced in [30]. The driver provides full dimming and does not employ electrolytic capacitors. However, two LFR flyback cells are used in each phase, thus, causing the circuit complexity to increase.

Recently, switched capacitor (SC) converters, also known as charge-pump ones, have been extensively used to drive power LEDs. They aggregate high power density and are able to keep the output current stable without the need of current sensors, which reduces design costs. In addition, LED dimming can be easily performed by varying the switching frequency [31]–[34]. According to [35], conventional SC-based topologies are defined as dc–dc converters composed only by switches and capacitors, which typically present low efficiency due to high current peaks that occur due to charging and discharging of existing SCs [36]–[38]. On the other hand, three-phase ac–ac converters using SCs have been proposed in [39] and [40] for power levels higher than 3 kW, whose efficiency is higher than 90%. Some authors also recommended the connection of a small inductor in series with the SC so that current peaks are minimized and efficiency is consequently improved. Such topologies are defined as resonant SC converters [41]–[43].

AC–DC charge-pump electronic ballasts were introduced in [44]–[47] for PFC purposes, although such approaches employ electrolytic capacitors. Charge-pump converters for LED drivers have been proposed in [33] and [48], which on the other hand do not require the aforementioned components. The topology implemented in [33] is able to achieve zero voltage switching (ZVS), where efficiency is 89.5% for a 22-W experimental prototype. However, the 120-Hz current ripple is 59%, which may lead to a percent flicker higher than the limit established as 10%

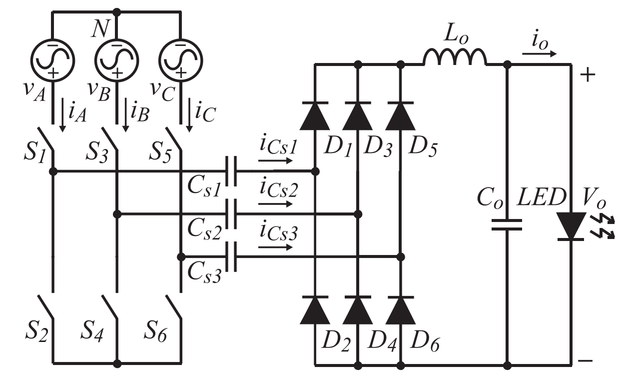

Fig. 1. Basic circuit of the three-phase resonant SC LED driver.

in [7]. It is worth to mention that this parameter may assume appreciable values up to 59% in this particular case [33]. The LED driver presented in [48] uses a low-pass LC (inductor–capacitor) filter in order to reduce the ripple current through the LEDs, which is equal to 65.6%.

Within this context, this paper proposes a three-phase LED driver based on resonant SC converters to drive a LED COB lamp rated at 216 W. The converter does not use electrolytic capacitors, also providing stable constant current through the LEDs and low percent flicker. The converter also allows LED dimming when varying the switching frequency, as high efficiency is achieved over the entire load range. An open-loop control system is also designed to demonstrate that it is possible to obtain low percent flicker without the need of complex closed-loop control.

II. Three-Phase Resonant SC LED Driver

Fig. 1 shows the basic configuration of the three-phase resonant SC LED driver without using an electromagnetic interference (EMI) filter. The converter consists of a three-phase full-bridge inverter; three SCs (C_{s1}, C_{s2}, and C_{s3}); one high-frequency diode bridge composed of six diodes ($\mathrm{D}_1-\mathrm{D}_6$); one output inductor L_o; one output filter capacitor C_o; and the LED array that behaves as a load. The output inductor L_o provides operation in continuous conduction mode, where the converter output side presents current source characteristic and allows the complete charging and discharging of the SCs. The output filter capacitor C_o is only used to mitigate high-frequency components.

A. Principle of Operation

Fig. 2 presents the time interval for which the converter operating stages can be defined. Time instant $t = t_0$ within $|v_{CN}| \geq |v_{AN}| \geq |v_{BN}|$ and $v_{CN} < 0$ is assumed for the initial analysis of the converter operation, since the three-phase voltages are assumed to be balanced. Fig. 3 shows the operating stages of the proposed converter. In order to simplify the analysis, switches S_1, S_3, and S_5 are driven simultaneously, and so are switches S_2, S_4, and S_6. However, it is worth to mention that $\mathrm{S}_1-\mathrm{S}_3-\mathrm{S}_5$ and $\mathrm{S}_2-\mathrm{S}_4-\mathrm{S}_6$ operate complementarily, where the

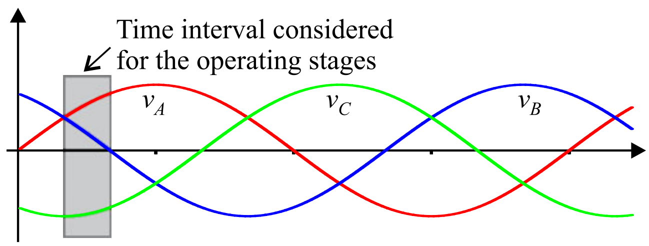

Fig. 2. Time interval considered for the analysis of the converter operating stages.

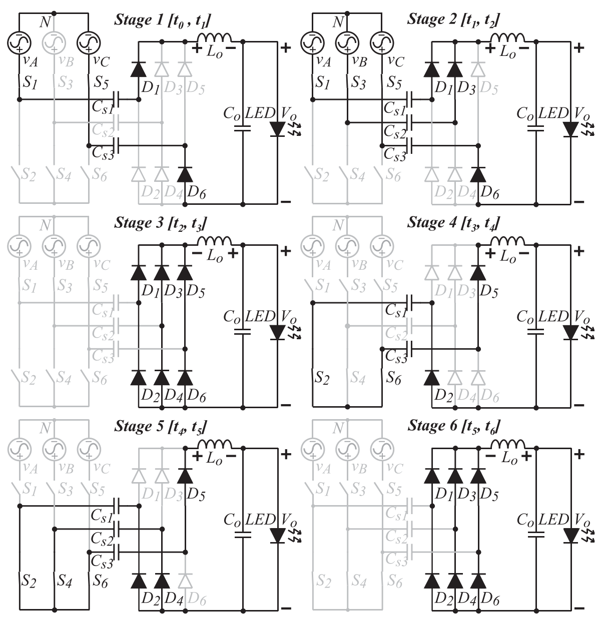

Fig. 3. Operating stages of the proposed LED driver (Black: turned ON components. Light gray: turned OFF components).

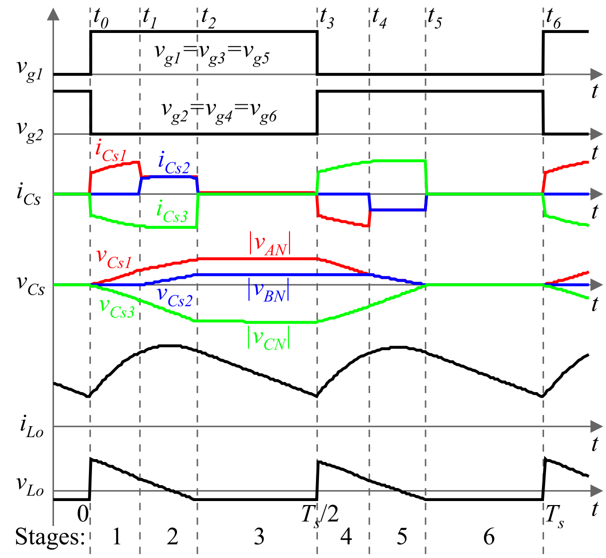

Fig. 4. Main theoretical waveforms of the proposed LED driver.

duty cycle is about 0.5. Fig. 4 shows the main theoretical waveforms of the proposed converter at t_0 for one switching period T_s ($T_s = 1/f_s$, where f_s is the switching frequency). The converter operation is analogous if any other initial time instant considered, according to the equivalent circuits and relevant waveforms discussed as follows. Besides, the drain-to-source on-resistances of metal oxide semiconductor field effect transistors (MOSFETs) and the intrinsic series resistances associated to inductors and capacitor are neglected in the analysis. Besides, all switches are turned ON hardly, although they are turned OFF under zero current switching (ZCS) and ZVS conditions.

Stage 1 $[t_0, t_1]$: Before instant t_0, the SCs are discharged. At t_0, switches S_1, S_3, and S_5 are turned ON, while S_2, S_4, and S_6 are turned OFF. During this stage, diodes D_1 and D_6 are forward biased and, consequently, capacitors C_{s1} and C_{s3} are charged. There is no current flowing through C_{s2} since the line voltage V_{AC} is higher than the line voltage V_{BC}.

Stage 2 $[t_1, t_2]$: The voltage across the capacitor C_{s1} equals the line voltage V_{AB} at t_1. Diode D_3 is forward biased and capacitor C_{s2} is charged.

Stage 3 $[t_2, t_3]$: The voltage across each SC equals the respective instantaneous phase voltage at t_2. During this stage, there is no current flow through the SCs. The voltage across inductor L_o becomes negative as energy is provided to the LEDs, thus, causing all diodes to be forwarded biased. It is also possible to notice that the SCs are connected to a common neutral point, as the voltage across them is equal to the phase voltage, which allows switches S_1, S_3, and S_5 to be turned OFF under ZVS condition.

Stage 4 $[t_3, t_4]$: At t_3, switches S_2, S_4, and S_6 are turned ON hardly, while S_1, S_3, and S_5 are turned OFF under ZCS and ZVS conditions. During this stage, diodes D_2 and D_5 are forward biased and, consequently, capacitors C_{s1} and C_{s3} start discharging. There is no current flowing through C_{s2} since the voltage across C_{s3} is higher than the voltage across C_{s2}.

Stage 5 $[t_4, t_5]$: The voltages across C_{s2} and C_{s3} are equal at t_4. Thus, diode D_4 is forward biased and capacitor C_{s2} starts discharging.

Stage 6 $[t_5, t_6]$: The SCs are fully discharged at t_5, while the current through them is null. Besides, inductor L_o provides energy to the LEDs and all diodes are forward biased. When this stage finishes, switches S_2, S_4, and S_6 are turned OFF under ZCS and ZVS conditions and a new switching cycle begins.

B. Calculation of SC Capacitances

Since the converter behaves as a three-phase balanced system, the phase voltages are defined as in (1)–(3), where V_M is the maximum input voltage and ω is the line angular frequency $\omega = 2\pi f_r$, since f_r is the line frequency

$$v_A(t) = V_M \cdot \sin(\omega t) \tag{1}$$

$$v_B(t) = V_M \cdot \sin\left(\omega t + \frac{2\pi}{3}\right) \tag{2}$$

$$v_C(t) = V_M \cdot \sin\left(\omega t - \frac{2\pi}{3}\right). \tag{3}$$

Considering that unity power factor is verified in the system phases, the input currents are given by (4)–(6), where I_M is the maximum input current and $K = I_M/V_M$

$$i_A(t) = I_M \cdot \sin(\omega t) = K \cdot v_A(t) \quad (4)$$

$$i_B(t) = I_M \cdot \sin\left(\omega t + \frac{2\pi}{3}\right) = K \cdot v_B(t) \quad (5)$$

$$i_C(t) = I_M \cdot \sin\left(\omega t - \frac{2\pi}{3}\right) = K \cdot v_C(t). \quad (6)$$

The input powers can be obtained by expressions (7)–(9)

$$p_A(t) = v_A(t) \cdot i_A(t) = K \cdot v_A^2(t) \quad (7)$$

$$p_B(t) = v_B(t) \cdot i_B(t) = K \cdot v_B^2(t) \quad (8)$$

$$p_C(t) = v_C(t) \cdot i_C(t) = K \cdot v_C^2(t). \quad (9)$$

On the other hand, considering that each SC is fully charged and discharged within one switching period, the input power can be determined as a function of the amount of energy associated to the charging and discharging of the SC as suggested in [32] and [49]. Thus, the input power for each phase can be given by (10)–(12) analogously to the procedure developed in [45] and [46], where $E_{Cs1}(t)$, $E_{Cs2}(t)$, and $E_{Cs3}(t)$ correspond to the amount of energy stored in SCs C_{s1}, C_{s2}, and C_{s3}, whose capacitances are equal and assumed as C_s

$$p_A(t) = 2 \cdot E_{Cs1}(t) \cdot f_s = C_s \cdot f_s \cdot v_A^2(t) \quad (10)$$

$$p_B(t) = 2 \cdot E_{Cs2}(t) \cdot f_s = C_s \cdot f_s \cdot v_B^2(t) \quad (11)$$

$$p_C(t) = 2 \cdot E_{Cs3}(t) \cdot f_s = C_s \cdot f_s \cdot v_C^2(t). \quad (12)$$

Comparing (10)–(12) with (7)–(9) and considering $K = C_s \cdot f_s$, it is possible to notice that the phase instantaneous powers in the proposed converter are equal to those regarding a balanced three-phase system with unity input power factor. It is then reasonable to assume that the resonant SC converter is able to provide PFC.

The total instantaneous input power $p_{\text{in}}(t)$ is equal to the sum of the phase input powers, i.e., summing (10)–(12) gives

$$p_{\text{in}}(t) = C_s f_s V_M^2 \cdot \left[\sin^2(\omega t) + \sin^2\left(\omega t + \frac{2\pi}{3}\right) + \sin^2\left(\omega t - \frac{2\pi}{3}\right)\right]. \quad (13)$$

According to [50], the sum of terms involving sinusoidal components represents a constant value $\left(\sin^2(\omega t) + \sin^2\left(\omega t + \frac{2\pi}{3}\right) + \sin^2\left(\omega t - \frac{2\pi}{3}\right) = \frac{3}{2}\right)$. Therefore, the instantaneous input power is given by (14)

$$p_{\text{in}}(t) = \frac{3}{2} C_s \cdot f_s \cdot V_M^2. \quad (14)$$

Equation (14) shows that the instantaneous input power is constant over time. By averaging (14), the average input power P_{in} can then be obtained as (15)

$$P_{\text{in}} = \frac{3}{2} C_s \cdot f_s \cdot V_M^2. \quad (15)$$

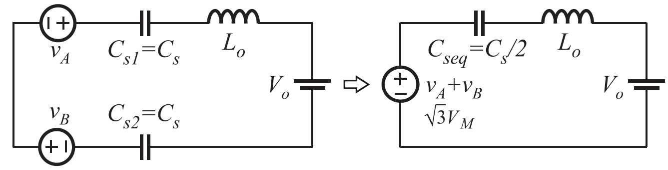

Fig. 5. Simplified equivalent circuit of the converter for $v_{AB} = \sqrt{3}V_M$.

On the other hand, the average output power P_o can be determined from (16), where η is the converter efficiency, V_o is the average output voltage, and I_o is the average output current

$$P_o = P_{\text{in}} \cdot \eta = V_o \cdot I_o. \quad (16)$$

The voltage across the LED array, i.e., the output voltage (V_o) is given by (17), where n is the number of series-connected LEDs in the array, V_{LED} is the LED forward voltage and R_{LED} is the LED intrinsic series resistance

$$V_o = n \cdot (V_{\text{LED}} + R_{\text{LED}} \cdot I_o). \quad (17)$$

Substituting (13) in (16) gives the average output power as in (18)

$$P_o = \tfrac{3}{2} C_s \cdot f_s \cdot V_M^2 \cdot \eta. \quad (18)$$

Expression (18) shows that the converter provides constant output power. In addition, the power transferred to the LED array does not depend on the voltage across it, i.e., V_o [32], [51]. Since LEDs present voltage source characteristic, the output voltage is practically constant and does not vary significantly with temperature [52]. Thus, the output current will be practically constant, assuming that V_M also is.

Isolating C_s in (18) gives the SC capacitance as in (19)

$$C_s = \frac{2}{3} \frac{P_o}{f_s \cdot V_M^2 \cdot \eta}. \quad (19)$$

C. Calculation of the Output Filter Inductance

The peak current through the inductor I_{Lopk} occurs when the line voltage associated to any two phases assumes the peak value, while the other phase voltage is null. Let us define $t = t_a$ as the instant at which $v_{AB}(t_a) = \sqrt{3}V_M$, $v_{AN}(t_a) = \frac{\sqrt{3}}{2}V_M$, $v_{BN}(t_a) = -\frac{\sqrt{3}}{2}V_M$, and $v_{CN}(t_a) = 0$. Fig. 5 shows the simplified representation of the converter at $t = t_a$ when switches S_1, S_3, and S_5 are ON, while the LED array is represented by V_o. Besides, there is no current flowing through C_{s3} since $v_{CN} = 0$.

By analyzing the circuit in Fig. 5 according to Kirchhoff's voltage law, expression (20) can be obtained, where C_{seq} is the equivalent capacitance for the parallel association of C_{s1} and C_{s2}, which is equal to $C_s/2$. Solving (20) gives (21), where I_{Lomin} is the minimum current through inductor L_o, and ω_o is the circuit resonance frequency defined as $\frac{1}{\sqrt{L_o C_{\text{seq}}}}$. In addition, the initial conditions for the differential equation in (20) are

$v_{C\text{seq}}(t_0) = 0$ and $i_{Lo}(t_0) = I_{\text{Lomin}}$

$$\sqrt{3}V_M = L_o C_{\text{seq}} \frac{d^2 v_{C\text{seq}}(t)}{dt^2} + v_{C\text{seq}}(t) + V_o \tag{20}$$

$$v_{C\text{seq}}(t) = (V_o - \sqrt{3}V_M) \cdot \cos(\omega_o t) + I_{Lo\min}\sqrt{\frac{L_o}{C_{\text{seq}}}} \cdot \sin(\omega_o t) + (\sqrt{3}V_M - V_o). \tag{21}$$

The instantaneous current through the inductor $i_{Lo}(t)$ can be obtained from (22)

$$i_{Lo}(t) = \sqrt{\frac{C_{\text{seq}}}{L_o}} \cdot (\sqrt{3}V_M - V_o) \cdot \sin(\omega_o t) + I_{Lo\min} \cdot \cos(\omega_o t). \tag{22}$$

Time instant t_2 is defined by (23) as

$$t_2 = \frac{\left(\cos^{-1}\left(-\frac{V_o}{c}\right) + \tan^{-1}\left(\frac{a}{b}\right)\right)}{\omega_o} \tag{23}$$

where

$$a = I_{Lo\min} \cdot \sqrt{\frac{L_o}{C_{\text{seq}}}};\ b = V_o - \sqrt{3}V_M;\ c = \sqrt{a^2 + b^2}. \tag{24}$$

The instant at which the inductor current is maximum, i.e., t_{pk} is given by (25)

$$t_{pk} = \frac{1}{\omega_{ob}} \cdot \tan^{-1}\left[\frac{(\sqrt{3}V_M - V_o) \cdot \sqrt{\frac{C_s}{2L_o}}}{I_{Lo\min}}\right]. \tag{25}$$

The output filter inductance can be determined from (26) and depends on t_2, which on the other hand also depends on L_o. Substituting (23) in (26) results in an expression whose analytical solution is not possible. However, parameter L_o can be determined by using a numerical method, which consists in setting the inductor current ripple Δi_{Lo} and an initial value for the inductance. The minimum current through inductor L_o is I_{Lomin}, whose value can be estimated by (27). Then, the maximum inductor current I_{Lpk} is obtained substituting t_{pk} in (22), while Δi_{Lo} is determined from (28). The value assumed by L_o is incremented until a fixed value for Δi_{Lo} is obtained

$$L_o = \frac{\left(\frac{1}{2f_s} - t_2\right) \cdot V_o}{i_{Lo}(t_2) - I_{Lo\min}} \tag{26}$$

$$I_{Lo\min} = I_o - \frac{\Delta i_{Lo}}{2} \tag{27}$$

$$\Delta i_{Lo} = I_{Lpk} - I_{Lo\min}. \tag{28}$$

III. Design Considerations

In order to evaluate the proposed converter performance in terms of reduced ripple current through the LEDs and low percent flicker without requiring a closed-loop control system, a 216-W prototype was implemented. Table I shows the design specifications of the resonant SC converter.

The converter has been designed to supply four series-connected COB LEDs, where each one of them has a series resistance $R_{\text{LED}} = 2.48\,\Omega$, forward voltage $V_{\text{LED}} = 26.59$ V, and rated current of 1.75 A. Then the output power and the output voltage can be calculated from (16) and (17), where $P_o = 216.51$ W and $V_o = 123.72$ V, respectively.

TABLE I
Design Parameters

Symbol	Parameter	Value
V_{in_rms}	rms phase input voltage	220 V ($V_M = 311$ V)
f_r	Line frequency	60 Hz
f_s	Switching frequency	50 kHz
Δi_{Lo}	Ripple current through inductor L_o	56%
I_o	Average output current	1.75 A
V_{LED}	LED forward voltage	26.59 V
R_{LED}	LED intrinsic series resistance	2.48 Ω
n	Number of series-connected LEDs	4

Considering that efficiency is 90%, the SC capacitance can be calculated from (19) as $C_s = 33.16$ nF, being $C_s = 33$ nF chosen as a commercial value.

Inductor L_o is designed considering that the current ripple is $\Delta i_{Lo} = 0.98$ A, i.e., 56% of the output current. The minimum current through L_o is obtained from (27). Using Δi_{Lo} and I_{Lomin}, it is possible to use a proper algorithm that allows calculating the inductance, which provides $L_o = 830\,\mu$H.

The output capacitor C_o is designed to operate at high frequencies according to the guidelines given in [53], where $C_o = 10\,\mu$F and eight multilayer ceramic capacitors rated at $10\,\mu$F/100 V each have been used in the prototype. It is worth to mention that the capacitances associated to such components is reduced as the voltage across them increases [54]. Two parallel-connected strings composed of four series-connected 10-μF capacitors have been used in this case, as the resulting equivalent capacitance is 20 μF. Considering that the involved capacitance is reduced by about 50% for the applied voltage, 10 μF is then obtained.

An input low-pass LC filter is added to reduce EMI levels. In order to achieve high input power factor over the entire dimming range, the input filter is designed according to the guidelines given in [55] considering an damping factor of 0.5 for the lowest operating frequency, i.e., 25 kHz, which corresponds to 50% of the rated output power.

MOSFETs are chosen for switches S_1-S_6 considering that the maximum voltage across them is equal to the peak line-to-line voltage. It is also worth to mention that all switches are turned OFF under ZCS–ZVS condition. However, according to [56], the turn-on losses in a given MOSFET correspond to one third of the switching losses, which on the other hand depend on the intrinsic capacitances associated to the switches. MOSFETs IRFB9N60A are then chosen in order to minimize the aforementioned losses as much as possible, where $C_{\text{oss}} = 49$ pF and $R_{D\text{Son}} = 750$ mΩ.

Switches $S_2-S_4-S_6$ present common-source connection, being a high-side bootstrap driver used to drive MOSFETs IR21844, where the dead time is 400 ns. All integrated circuits employ a same gating signal whose duty cycle is about 0.5 and the switching frequency varies from 25 to 50 kHz in order to achieve LED dimming. For general-purpose lighting applications, it is worth to mention that the converter should employ frequency

TABLE II
PROTOTYPE PARAMETERS AND COMPONENTS

Symbol	Parameter/Component	Value/Type
$L_{f1} - L_{f3}$	Filter inductors	5.5 mH/core EE25
$C_{f1} - C_{f3}$	Filter capacitors	330 nF/EPCOS B32694/P9 film capacitor
$S_1 - S_6$	MOSFETs	IRFB9N60A
$C_{s1} - C_{s3}$	Switched capacitors	33 nF / WIMA MKP 10 film capacitor
$D_1 - D_6$	Output diodes	MUR460
L_o	Output filter inductor	830 μH/core EE30/14
C_o	Output filter capacitors	8 × 10 μF/multilayer ceramic capacitor
	MOSFET drivers	IR21844

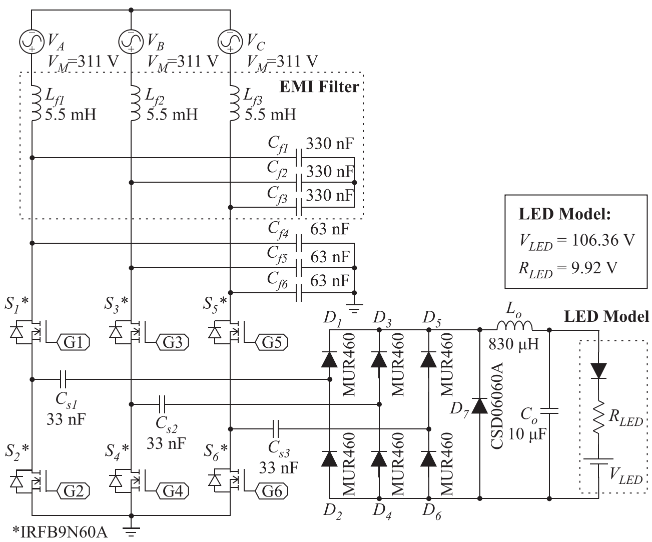

Fig. 6. Power stage of the three-phase resonant SC converter.

modulation to compensate variations of the input voltage. Table II presents the parameters and components used in the implementation of the experimental prototype.

Fig. 6 represents the power stage of the three-phase converter. Three polypropylene capacitors (C_{f4}, C_{f5}, and C_{f6}) rated at 63 nF/630 V are added to prevent eventual overvoltage across the MOSFETs. Besides, a SiC (silicon carbide) diode (D_7) is also connected in parallel with the rectifier bridge diodes to avoid them to be forward biased when inductor L_o is discharged. Since the forward voltage across D_7 is lower than the sum of voltages across two series-connected diodes, it is supposed to be forward biased first, thus, preventing the remaining diodes to be on. Therefore, it is possible to reduce conduction losses considering that the current flows through less components. Besides, switching losses are also minimized since SiC diodes have reverse recovery times less than those regarding the ultrafast silicon diodes MUR460 used in the rectifier bridge.

IV. EXPERIMENTAL RESULTS

Fig. 7 shows the input voltage and input current in phase A, and also the output voltage and output current at rated load condition, where power factor is 0.996 and the current total harmonic distortion (THD) is 4.22%. Besides, the rms values of the voltage and current in phase A are 217.9 V and 373 mA,

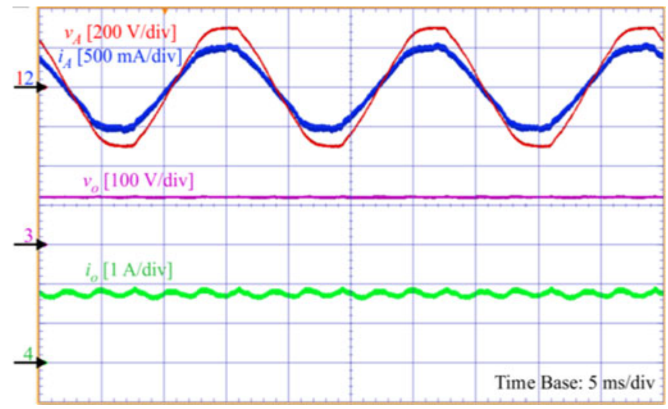

Fig. 7. Input voltage (v_A) and input current (i_A) in phase A; voltage (v_o) and current waveforms (i_o) in the LEDs at rated load condition.

TABLE III
PARAMETERS MEASURED WITH POWER ANALYZER PA4000

	Input			Output	
	Ch1	Ch2	Ch3		Ch4
$V_{\rm rms}$	214.42 V	220.82 V	219.65 V	$V_{\rm dc}$	125.27 V
$A_{\rm rms}$	374.25 mA	371.83 mA	372.90 mA	$A_{\rm dc}$	1.7712 A
Watt	79.541 W	81.660 W	81.247 W	*Watt*	221.90 W
PF	0.9912	0.9946	0.9919		
$A_{\rm THD}$	3.5670%	3.7509%	4.3456%		

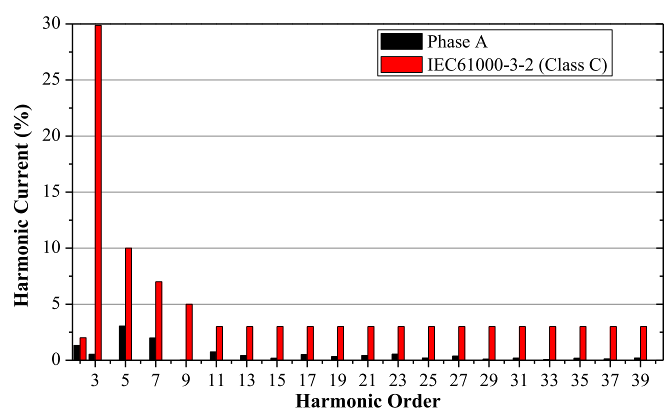

Fig. 8. Harmonic content of the input current in phase A and limits imposed by standard IEC 61000-3-2 for class C equipment.

respectively. On the other hand, the output voltage is 121.1 V and the output current is 1.755 A, while the current ripple at 360 Hz is 174 mA, thus, corresponding to 10% of the average output current.

In order to measure the converter efficiency, power analyzer model PA4000 manufactured by Tektronix was employed. Channels 1, 2, and 3 are used to measure some relevant quantities in the converter input side, while channel 4 is connected to the output side. Table III shows that the three-phase converter presents high input power factor and low current THD. Besides, overall efficiency is 91.5% for the rated load condition.

Fig. 8 shows the harmonic content of the input current in phase A. It is worth to mention that the converter can be considered

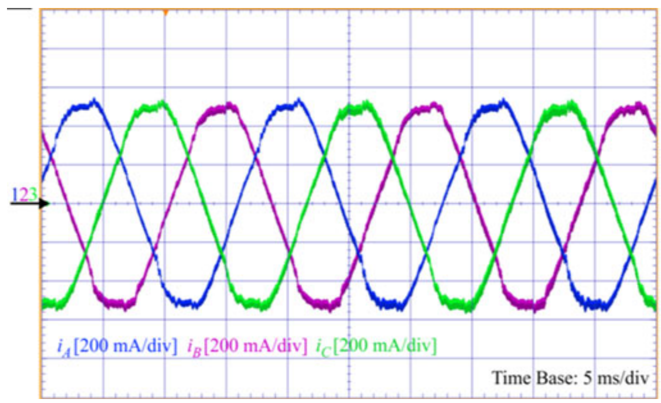

Fig. 9. Input currents at rated load condition.

as class A equipment since it is a balanced three-phase system. It may also belong to class C because it consists in lighting equipment [30]. The harmonic content of the input current is then compared with the limits imposed by IEC Std. 61000-3-2:2014 to class C equipment, which is the most restrictive one. It can be seen that the converter complies with the aforementioned limits, as well as those established for class A, which have been omitted in the graph since they are represented in terms of absolute values, and not as a percentage of the fundamental component. Since the converter is supplied by nearly balanced voltages, similar results are expected for the remaining phases.

Fig. 9 presents the input currents, which are phase-shifted by 120° from each other and are nearly sinusoidal, thus, showing that the converter allows PFC.

Fig. 10 represents the voltage and current waveforms regarding SC C_{s1}. Fig. 10(a) shows that the maximum voltage across it is equal to that regarding its respective phase voltage. It can be seen in Fig. 10(b) that the capacitor is fully charged and discharged over one switching period, thus, allowing PFC.

Fig. 11 shows the drive signals applied to switches $S_1 - S_3 - S_5$ (v_{g1}) and $S_2 - S_4 - S_6$ (v_{g2}), as well as the detailed view of voltage and current waveforms representing the commutation of S_2. It can be seen that the switch is turned OFF under ZCS and ZVS condition, with consequent reduction of switching losses and increase of converter efficiency.

LED dimming is achieved when varying the switching frequency. Fig. 12 presents the behavior of the output power as a function of the switching frequency. It can be seen that reducing the switching frequency from 50 kHz to 25 kHz causes the rated output power to be reduced from 100% to 50%, respectively. If the output power is further reduced, the switching frequency is supposed to assume values within the hearing range, and consequently the output power has been limited to 50% in this case.

Fig. 13 shows the recommended operating area defined according to the percent flicker or modulation (%) and ripple frequency [7]. The percent flicker is measured using photodiode model BPW21R, whose sensitivity curve is close to that regarding the human eye [57]. Besides, it is worth to mention that the output current of the three-phase resonant SC converter presents a ripple current frequency of 360 Hz, for which the

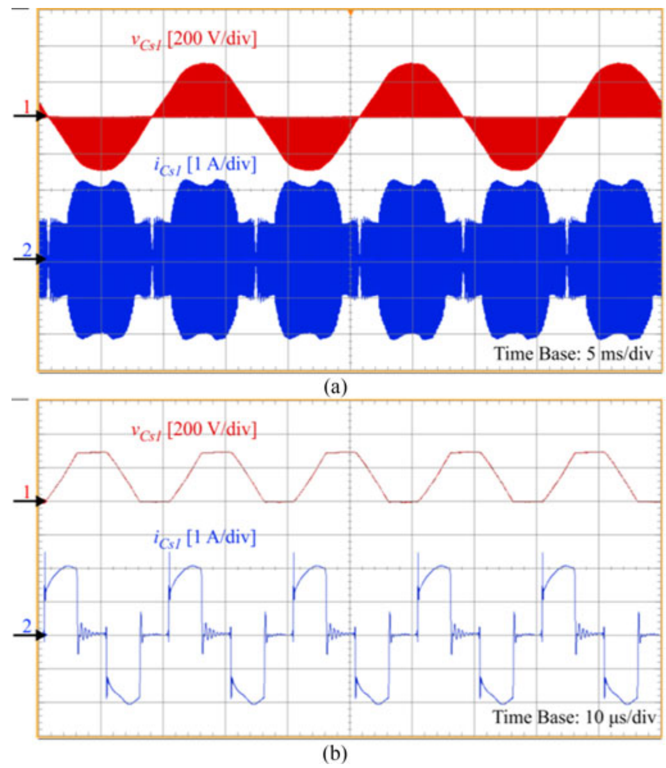

Fig. 10. Voltage (v_{Cs1}) and current (i_{Cs1}) waveforms in SC C_{s1}: (a) Low-frequency view anb (b) high-frequency view.

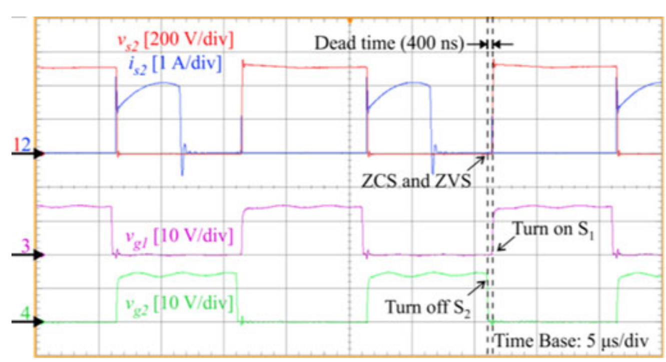

Fig. 11. Gating signals applied to the active switches and detailed view of commutation in S_2.

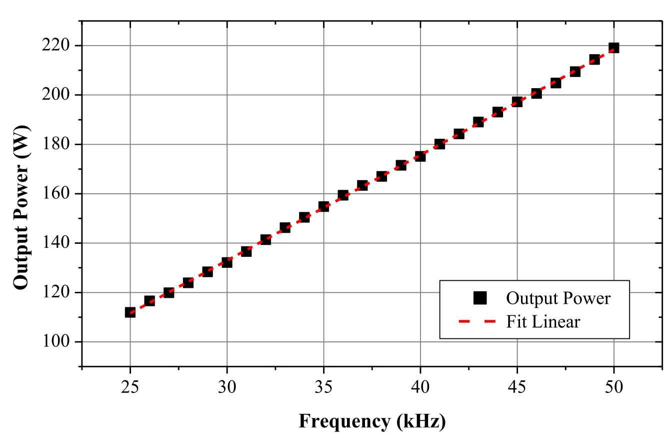

Fig. 12. Output power variation as a function of the switching frequency.

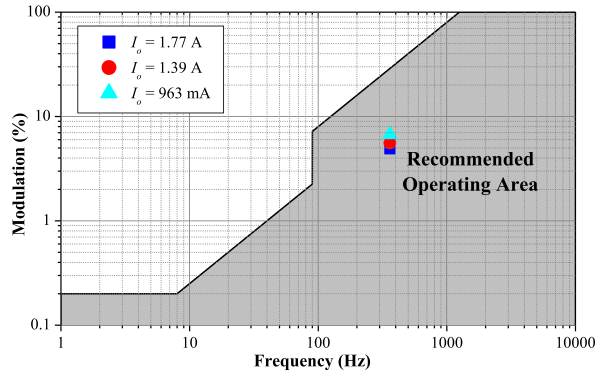

Fig. 13. Recommended operating area in terms of percent flicker [modulation (%)] as a function of the ripple frequency [7].

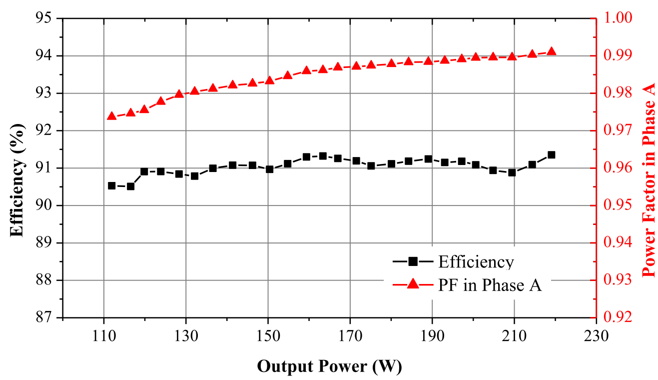

Fig. 14. Efficiency and power factor in phase A as a function of the output power.

maximum recommended percent flicker is 29% [7]. Percent values of 4.97%, 5.64%, and 6.83% have been obtained for output currents rated at 1.77 A, 1.39 A, and 963 mA, respectively. It can be stated that the converter output power can be reduced up to 50% while maintaining the percent flicker at 360 Hz within the IEEE recommended limits. The proposed converter does not employ any specific closed-loop control technique, thus making it a simple approach.

Fig. 14 represents the curves of the converter efficiency and power factor in phase A as function of the output power. It can be seen that overall efficiency is higher than 90% over the entire load range, while it is 90.5% at nearly half load condition (111.93 W). It is also worth to mention that all switches are turned OFF under ZCS and ZVS conditions over the entire load range. Power factor remains higher than 0.97 and efficiency does not seem to be drastically affected as the switching frequency varies. The current THD is lower than 6% over the entire dimming range. Since the converter is supplied three-phase balanced voltages, similar results have also been achieved for the remaining phases. It is then reasonable to state that the converter allows dimming with high power factor and low harmonic distortion in accordance with the limits established by standard IEC 61000-3-2:2014 [58].

Table IV shows a brief comparison associated to distinct LED drivers involving efficiency, THD, percent flicker, current ripple, and dimming range. It can be seen that the configuration proposed in this work presents the best performance in terms of rated power, efficiency, percent flicker, and current ripple.

TABLE IV
COMPARISON AMONG LED DRIVERS

	Proposed LED driver	References			
		[9]	[27]	[30]	[33]
Number of phases	Three-phase	Single-phase	Three-phase	Three-phase	Single-phase
Power	216 W	90 W	54 W	90 W	22 W
Efficiency (η)	91%	84%	77%	88%	89.5%
THD	4.22%	14.5%	6.72%	5.71%	1.61%
Percent flicker	4.97% (at 360 Hz)	65% (at 120 Hz)	Not evaluated	15% (at 300 Hz)	Not evaluated
Current ripple	10%	140%	Not evaluated	About 28%	59%
Dimming ability	Yes (50–100%)	Not evaluated	Not evaluated	Yes (0–100%)	Yes (60–100%)

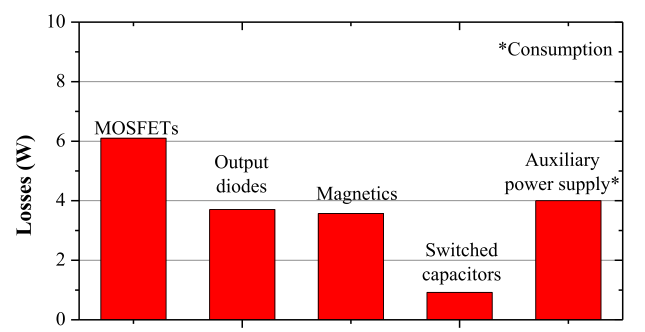

Fig. 15. Estimated losses in the power stage elements under rated load condition.

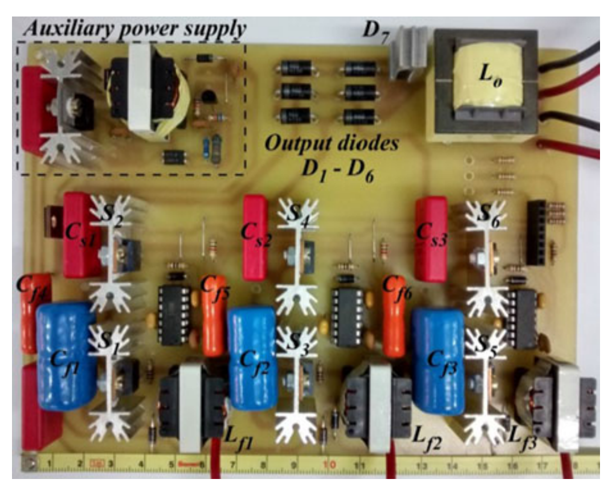

Fig. 16. Experimental prototype.

Fig. 15 shows the estimated losses in the main components of the power stage. It is worth to mention that losses were properly estimated numerically and the resulting theoretical efficiency is about 92% in this case, which is close to the value obtained when evaluating the experimental prototype. Besides, it can be seen that the existing losses are mainly due to MOSFETs and the output diodes.

Fig. 16 presents the experimental prototype, where the absence of electrolytic capacitors is clearly noticed.

V. Conclusion

This paper has proposed a LED driver based on a three-phase resonant SC converter. Experimental results obtained from a 216-W prototype have shown that the converter overall efficiency is 91% at rated load condition, while power factor is higher than 0.97 and percent flicker is lower than 7% for the dimming range from 50% to 100% of the rated output power. Besides, lifespan is expanded considering the absence of conventional electrolytic capacitors in the developed prototype.

Therefore, the introduced three-phase resonant SC converter comes as a prominent solution to drive LEDs, since it aggregates long useful lifer, high efficiency, low ripple current, and low percent flicker using a simple circuit that does not require a closed-loop control system.

Further improvements can be obtained by using a microcontroller in order to adjust the switching frequency according to the amplitudes of the input phase voltages. Thus, the output power can be maintained constant even though the grid voltage comes to vary over a wide range.

Acknowledgment

The authors would like to thank Mechatronics Research Group (GPEM) and Federal Institute of Ceará (IFCE–Campus Sobral), where the prototype was developed and evaluated.

References

[1] N. Vakrilov, A. Andonova, and N. Kafadarova, “Study of high power COB LED modules with respect to topology of chips,” in *Proc. 38th Int. Spring Semin. Electron. Technol.*, 2015, pp. 108–113.

[2] Lumileds, “LUXEON CoB core range (Gen 3): Uniform, high-efficacy and easy-to-design array,” 2016. [Online]. Available: http://www.lumileds.com/uploads/600/DS162-pdf [Accessed: 24-Feb-2016].

[3] Lumileds, “LUXEON CoB compact range: Unsurpassed light quality and CBCP due to samll LES,” 2015. [Online]. Available: http://www.lumileds.com/uploads/546/DS139-pdf [Accessed: 24-Feb-2016].

[4] Y. X. Qin, H. S. H. Chung, D. Y. Lin, and S. Y. R. Hui, “Current source ballast for high power lighting emitting diodes without electrolytic capacitor,” in *Proc. 34th Annu. Conf. IEEE Ind. Electron. Soc.*, 2008, pp. 1968–1973.

[5] A. Wilkins, J. Veitch, and B. Lehman, “LED lighting flicker and potential health concerns: IEEE standard PAR1789 update,” in *Proc. IEEE Energy Convers. Congr. Expo.*, 2010, pp. 171–178.

[6] B. Lehman and A. J. Wilkins, “Designing to mitigate effects of flicker in LED lighting: Reducing risks to health and safety,” *IEEE Power Electron. Mag.*, vol. 1, no. 3, pp. 18–26, Sep. 2014.

[7] *IEEE Recommended Practices for Modulating Current in High-Brightness LEDs for Mitigating Health Risks to Viewers*, IEEE Std 1789-2015, Jun. 2015, pp. 1–80.

[8] B. Wang, X. Ruan, K. Yao, and M. Xu, “A method of reducing the peak-to-average ratio of LED current for electrolytic capacitor-less AC-DC drivers,” *IEEE Trans. Power Electron.*, vol. 25, no. 3, pp. 592–601, Mar. 2010.

[9] F. J. Nogueira, T. S. Gomide, E. S. Silva, M. F. Braga, and H. A. C. Braga, “Low frequency led driver based on the Ćuk converter applied to street lighting luminaires,” in *Proc. 15th Brazilian Power Electron. Conf. 1st South. Power Electron. Conf.*, 2015, pp. 1–6.

[10] C. S. Wong, K. H. Loo, Y. M. Lai, M. H. L. Chow, and C. K. Tse, “An alternative approach to LED driver design based on high-voltage driving,” *IEEE Trans. Power Electron.*, vol. 31, no. 3, pp. 2465–2475, Mar. 2016.

[11] L. G. L. Gu, X. R. X. Ruan, M. X. M. Xu, and K. Y. K. Yao, “Means of eliminating electrolytic capacitor in AC/DC power supplies for LED lightings,” *IEEE Trans. Power Electron.*, vol. 24, no. 5, pp. 1399–1408, May 2009.

[12] S. Zhao, X. Ge, X. Wu, and J. Zhang, “Analysis and design considerations of two-stage AC- DC LED driver without electrolytic capacitor,” in *Proc. IEEE Energy Convers. Congr. Expo.*, Sep. 2014, no. 2013, pp. 2606–2610.

[13] S. Li, S.-C. Tan, C. K. Lee, E. Waffenschmidt, S. Y. R. Hui, and C. K. Tse, “A survey, classification, and critical review of light-emitting diode drivers,” *IEEE Trans. Power Electron.*, vol. 31, no. 2, pp. 1503–1516, Feb. 2016.

[14] P. Almeida, D. Camponogara, M. Dalla Costa, H. Braga, and J. Alonso, “Matching LED and driver life spans: A review of different techniques,” *IEEE Ind. Electron. Mag.*, vol. 9, no. 2, pp. 36–47, Jun. 2015.

[15] J. M. Alonso, J. Viña, D. G. Vaquero, G. Martínez, and R. Osorio, “Analysis and design of the integrated double buck-boost converter as a high-power-factor driver for power-led lamps,” *IEEE Trans. Ind. Electron.*, vol. 59, no. 4, pp. 1689–1697, Apr. 2012.

[16] B. Poorali and E. Adib, “Analysis of the integrated SEPIC-flyback converter as a single-stage single-switch power-factor-correction LED driver,” *IEEE Trans. Ind. Electron.*, vol. 63, no. 6, pp. 3562–3570, Jun. 2016.

[17] Y. Wang, J. Huang, W. Wang, and D. Xu, “A single-stage single-switch LED driver based on class-E converter,” *IEEE Trans. Ind. Appl.*, vol. 53, no. 3, pp. 2618–2626, May/Jun. 2016.

[18] W. Chen and S. Y. R. Hui, “Elimination of an electrolytic capacitor in AC/DC light-emitting diode (LED) driver with high input power factor and constant output current,” *IEEE Trans. Power Electron.*, vol. 27, no. 3, pp. 1598–1607, Mar. 2012.

[19] S. Wang, X. Ruan, K. Yao, S. C. Tan, Y. Yang, and Z. Ye, “A flicker-free electrolytic capacitor-less AC-DC LED driver,” *IEEE Trans. Power Electron.*, vol. 27, no. 11, pp. 4540–4548, Nov. 2012.

[20] Y. Zhang and K. Jin, “A single-stage electrolytic capacitor-less AC/DC LED Driver,” in *Proc. Int. Electron. Appl. Conf. Expo.*, 2014, pp. 881–886.

[21] P. Fang, Y. F. Liu, and P. C. Sen, “A flicker-free single-stage offline LED driver with high power factor,” *IEEE J. Emerg. Sel. Topics Power Electron.*, vol. 3, no. 3, pp. 654–665, Sep. 2015.

[22] P. Fang and Y. F. Liu, “An electrolytic capacitor-free single stage Buck-Boost LED driver and its integrated solution,” in *Proc. IEEE Appl. Power Electron. Conf. Expo.*, Mar. 2014, pp. 1394–1401.

[23] Y. Qiu, L. Wang, H. Wang, Y.-F. Liu, and P. Sen, “Bipolar ripple cancellation method to achieve single-stage electrolytic-capacitor-less high-power LED driver,” *IEEE J. Emerg. Sel. Topics Power Electron.*, vol. 3, no. 3, pp. 698–713, Sep. 2015.

[24] D. Camponogara *et al.*, “Optimized cascade structure applied to LED street lighting,” in *Proc. 38th Annu. Conf. IEEE Ind. Electron. Soc.*, 2012, no. 1, pp. 4581–4585.

[25] D. Camponogara, G. F. Ferreira, A. Campos, M. A. Dalla Costa, and J. Garcia, “Offline LED driver for street lighting with an optimized cascade structure,” *IEEE Trans. Ind. Appl.*, vol. 49, no. 6, pp. 2437–2443, Nov./Dec. 2013.

[26] D. Camponogara, D. R. Vargas, M. A. Dalla Costa, J. M. Alonso, J. Garcia, and T. Marchesan, “Capacitance reduction with an optimized converter connection applied to LED Drivers,” *IEEE Trans. Ind. Electron.*, vol. 62, no. 1, pp. 184–192, Jan. 2015.

[27] M. R. Mendonça, E. M. Sá Jr., R. P. Coutinho, and F. L. M. Antunes, “AC-DC single-switch three-phase converter with peak current control for power LEDs,” in *Proc. 11th IEEE/IAS Int. Conf. Ind. Appl.*, 2014, p. 1–6.

[28] C. K. Alexander and M. N. O. Sadiku, *Fundamentals of Electric Circuits*, 3rd ed. New York, NY, USA: McGraw-Hill, 2004.

[29] D. W. Hart, *Power Electronics*, 1st ed. New York, NY, USA: McGraw-Hill, 2010.

[30] I. Castro, D. G. Lamar, M. Arias, J. Sebastián, and M. M. Hernando, “Three phase converter with galvanic isolation based on loss-free resistors for HB-LED lighting applications,” in *Proc. IEEE Appl. Power Electron. Conf. Expo.*, 2016, pp. 822–829.

[31] E. M. Sá Jr., P. H. A. Miranda, E. E. dos Santos Filho, and F. L. M. Antunes, “DC/DC converter with switched capacitor applied for power equalization in LED clusters,” *Eletrôn. Potên.*, vol. 18, no. 3, pp. 1100–1108, 2013.

[32] E. E. dos Santos Filho, P. H. A. Miranda, E. M. Sá Jr., and F. L. M. Antunes, “A LED driver with switched capacitor,” *IEEE Trans. Ind. Appl.*, vol. 50, no. 5, pp. 3046–3054, Sep./Oct. 2014.

[33] R. L. dos Santos, R. P. Coutinho, K. C. A. de Souza, and E. M. Sá Jr., “A dimmable charge-pump ZVS led driver with PFC,” in *Proc. 13th IEEE Brazilian Power Electron. Conf. 1st Southern Power Electron. Conf.*, 2015, pp. 1–6.

[34] A. F. Rocha, E. R. Marques, C. E. A. Silva, and E. M. Sá Jr., "A step-up converter with switched capacitor using a small inductor in CCM to drive power leds," in *Proc. 13th IEEE Brazilian Power Electron. Conf. 1st Southern Power Electron. Conf.*, 2015, pp. 1–5.
[35] M. Martins, M. S. Perdigao, A. M. S. Mendes, R. A. Pinto, and J. M. Alonso, "Analysis, design and experimentation of a dimmable resonant-switched-capacitor LED driver with variable inductor control," *IEEE Trans. Power Electron.*, vol. 32, no. 4, pp. 3051–3062, Apr. 2016.
[36] A. Ioinovici, "Switched-capacitor power electronics circuits," *IEEE Circuits Syst. Mag.*, vol. 1, no. 3, pp. 37–42, Jul.–Sep. 2001.
[37] G. Wu, X. Ruan, and Z. Ye, "Nonisolated high step-Up DC-DC converters adopting switched-capacitor cell," *IEEE Trans. Ind. Electron.*, vol. 62, no. 1, pp. 383–393, Jan. 2015.
[38] W. Qian, D. Cao, J. G. Cintron-Rivera, M. Gebben, D. Wey, and F. Z. Peng, "A switched-capacitor DC-DC converter with high voltage gain and reduced component rating and count," *IEEE Trans. Ind. Appl.*, vol. 48, no. 4, pp. 1397–1406, Jul./Aug. 2012.
[39] T. B. Lazzarin, R. L. Andersen, and I. Barbi, "A switched-capacitor three-phase AC-AC converter," *IEEE Trans. Ind. Electron.*, vol. 62, no. 2, pp. 735–745, Feb. 2015.
[40] M. D. Vecchia, T. B. Lazzarin, and I. Barbi, "A three-phase AC-AC converter in open-delta connection based on switched capacitor principle," *IEEE Trans. Ind. Electron.*, vol. 62, no. 10, pp. 6035–6041, Oct. 2015.
[41] Y. P. B. Yeung, K. W. E. Cheng, S. L. Ho, K. K. Law, and D. Sutanto, "Unified analysis of switched-capacitor resonant converters," *IEEE Trans. Ind. Electron.*, vol. 51, no. 4, pp. 864–873, Aug. 2004.
[42] K. K. Law, K. W. E. Cheng, and Y. P. B. Yeung, "Design and analysis of switched-capacitor-based step-up resonant converters," *IEEE Trans. Circuits Syst. I, Reg. Papers*, vol. 52, no. 5, pp. 943–948, May 2005.
[43] Y.-S. Lee and Y.-Y. Chiu, "Zero-current-switching switched-capacitor bidirectional DC–DC converter," *IEE Proc.—Elect. Power Appl.*, vol. 152, no. 6, p. 1525–1530, 2005.
[44] W. Chen, F. C. Lee, and T. Yamauchi, "An improved 'charge pump' electronic ballast with low THD and low crest factor," *IEEE Trans. Power Electron.*, vol. 12, no. 5, pp. 867–875, Sep. 1997.
[45] J. Qian, F. C. Y. Lee, and T. Yamauchi, "Current-source charge-pump power-factor-correction electronic ballast," *IEEE Trans. Power Electron.*, vol. 13, no. 3, pp. 564–572, May 1998.
[46] J. Qian, F. C. Lee, and T. Yamauchi, "Charge pump power-factor-correction dimming electronic ballast," *IEEE Trans. Power Electron.*, vol. 14, no. 3, pp. 461–468, May 1999.
[47] R. Lin, H. Liu, and H. Shih, "AC-Side CCM CS-CP-PFC electronic ballast," *IEEE Trans. Power Electron.*, vol. 22, no. 3, pp. 789–796, May 2007.
[48] E. E. dos Santos Filho, E. M. Sa Jr., R. L. Dos Santos, P. A. Miranda, and F. L. M. Antunes, "Single stage switched capacitor LED driver with high power factor and reduced current ripple," in *Proc. IEEE Appl. Power Electron. Conf. Expo.*, 2015, pp. 906–912.
[49] E. E. dos Santos Filho, F. L. M. Antunes, E. M. Sá Jr., and R. L. dos Santos, "Off-line a single-stage resonant switched capacitor high- power-factor led driver," in *Proc. 11th IEEE/IAS Int. Conf. Ind. Appl.*, 2014, pp. 6–11.
[50] A. E. Fitzgerald, *Electric Machinery*. 6th ed. New York, NY, USA: McGraw-Hill, 2003.
[51] E. E. dos Santos Filho, F. L. M. Antunes, E. M. Sá Jr., R. L. dos Santos, and P. Miranda, "Off-line a single-stage resonant switched capacitor high-power-factor LED driver," in *Proc. 11th IEEE/IAS Int. Conf. Ind. Appl.*, 2014, pp. 6–11.
[52] E. M. Sa, F. L. M. Antunes, and A. J. Perin, "Junction temperature estimation for high power light-emitting diodes," in *Proc. 2007 IEEE Int. Symp. Ind. Electron.*, Jun. 2007, pp. 3030–3035.
[53] Cirrus Logic, "AN376 single stage output ripple current and the effect on load current in a LED driver," AN376REV2, Jul. 2013.
[54] TDK, "MLCC C5750X7S2A106M230KE 10uF 100 V," 2016 [Online]. Available: https://product.tdk.com/info/en/documents/chara_sheet/C5750X7S2A106M230KE.pdf [Accessed: 13-Jul-2016].
[55] R. L. Ozenbaugh, *EMI Filter Design*, 2nd ed. New York, NY, USA: Marcel Dekker, 2001.
[56] M. K. Kazimierczuk, *Pulse-Width Modulated DC-DC Power Converters*. Hoboken, NJ, USA: Wiley, 2008.
[57] P. S. Almeida V. C. Bender, H. A. C. Braga, M. A. Dalla Costa, T. B. Marchesan, and J. M. Alonso, "Static and dynamic photoelectrothermal modeling of LED lamps including low-frequency current ripple effects," *IEEE Trans. Power Electron.*, vol. 30, no. 7, pp. 3841–3851, Jul. 2015.
[58] *Electromagnetic Compatibility (EMC) - Part 3-2: Limits for Harmonic Current Emissions (Equipment Input Current ≤ 16 A per Phase)*, IEC 61000-3-2:2014, 2014.

Ronaldo P. Coutinho was born in Fortaleza, Brazil. He received the Technologist degree in industrial mechatronics from the Federal Institute of Ceará, Sobral, Brazil, in 2010, the B.Sc. degree in mathematics and the Specialist degree in mathematics teaching from the State University Vale do Acaraú, Sobral, Brazil, in 2011 and 2014, respectively, and the M.S. degree in electrical and computer engineering from the Federal University of Ceará, Sobral, in 2016.

Since 2014, he has been a Researcher with the Mechatronics Research Group (GPEM), Federal Institute of Ceará, Sobral. His research interests include LED drivers, power factor correction circuits, and single-phase and three-phase converters.

Kleber C. A. de Souza was born in Campina Grande, Brazil. He received the B.S. and M.S. degrees in electrical engineering from the Federal University of Ceará, Fortaleza, Brazil, in 1999 and 2003, respectively, and the Ph.D. degree in electrical engineering from the Federal University of Santa Catarina, Florianópolis, Brazil, in 2009.

Since 2008, he has been a Professor at the Federal Institute of Ceará, Sobral, Brazil, where he coordinates the Electrical System Laboratory. His research interests include electronic electrical energy generation, power factor correction circuits, dc–dc converters and their applications to renewable energy systems, smart grids, and LED drivers.

Prof. Souza is Member of the Brazilian Power Electronics Society (SOBRAEP).

Fernando L. M. Antunes (M'91) was born in Cascavel, Brazil. He received the B.Sc. degree in electrical engineering from the Federal University of Ceará, Brazil, in 1978, the B.Sc. degree in business and administration from the State University of Ceará, Brazil, in 1982, the M.Sc. degree in electrical engineering from the University of Sao Paulo, Brazil, in 1980, and the Ph.D. degree in electrical engineering from Loughborough University of Technology, U.K., in 1991.

He is a Professor at the Federal University of Ceará, Fortaleza, Brazil, where he coordinates the Power Electronics Group. His research fields include multilevel converters, inverters, dc–dc converters and their application to renewable energy systems, and LED drivers.

Prof. Antunes is a Member of the Brazilian Power Electronics Society (SOBRAEP), IEEE Power Electronics Society, and IEEE Industrial Electronics Society. From 2009 to 2011, he was President of SOBRAEP.

Edilson Mineiro Sá Jr. was born in Fortaleza, Brazil. He received the B.S. and M.S. degrees in electrical engineering from the Federal University of Ceará, Fortaleza, Brazil, in 1999 and 2004, respectively, and the Ph.D. degree from the Federal University of Santa Catarina, Florianopolis, Brazil, in 2010.

Since 2008, he has been a Professor at the Federal Institute of Ceará, Sobral, Brazil, where he coordinates the Mechatronics Research Group (GPEM). His research interests include electronic ballasts, power factor correction circuits, dc–dc converters and their application to renewable energy systems, and LED drivers.

Prof. Sá is a Member of the Brazilian Power Electronics Society (SOBRAEP).